ORIGINAL PAPER

CrossMark

Solvent Free Synthesis of PdZn/TiO$_2$ Catalysts for the Hydrogenation of CO$_2$ to Methanol

Hasliza Bahruji[1] · Jonathan Ruiz Esquius[1] · Michael Bowker[1,2] · Graham Hutchings[1] · Robert D. Armstrong[1] · Wilm Jones[1,2]

Abstract
Catalytic upgrading of CO$_2$ to value-added chemicals is an important challenge within the chemical sciences. Of particular interest are catalysts which are both active and selective for the hydrogenation of CO$_2$ to methanol. PdZn alloy nanoparticles supported on TiO$_2$ via a solvent-free chemical vapour impregnation method are shown to be effective for this reaction. This synthesis technique is shown to minimise surface contaminants, which are detrimental to catalyst activity. The effect of reductive heat treatments on both structural properties of PdZn/TiO$_2$ catalysts and rates of catalytic CO$_2$ hydrogenation are investigated. PdZn nanoparticles formed upon reduction showed high stability towards particle sintering at high reduction temperature with average diameter of 3–6 nm to give 1710 mmol kg^{-1} h of methanol. Reductive treatment at high temperature results in the formation of ZnTiO$_3$ as well as PdZn, and gives the highest methanol yield.

Keywords CO$_2$ hydrogenation · Methanol · PdZn alloy · Green methanol · Hydrogen storage

1 Introduction

Atmospheric CO$_2$ levels continue to increase, now inexorably linked with anthropogenic emissions and climate change [1]. The scientific community therefore faces a major challenge; to act collectively in curtailing global CO$_2$ emissions whilst simultaneously exploring low-environmental impact routes to generating energy. Although usually considered a waste product, CO$_2$ can be a sustainable carbon source for fuel synthesis. Provided that hydrogen is also generated from sustainable sources, the hydrogenation of CO$_2$ to methanol could underpin the oft cited methanol economy, providing a non-fossil fuel derived energy storage, fuel and chemical feedstock [2]. Ideally, H$_2$ would be produced via electrolysis of water utilising renewable energy. Whilst hydrogen is itself a good energy carrier, with high energy density per mass and clean combustion, it has low volume energy density. An integrated approach, with H$_2$ generation and CO$_2$ hydrogenation processes/plants in close physical proximity would be advantageous [3].

The utilisation of CO$_2$ as a carbon source for methanol synthesis has been studied extensively, though is yet to be commercialised on a large scale. Methanol is therefore still produced on a world scale from synthesis gas (at 200–300 °C, 50–100 bar), which is itself the product of methane steam reforming (at *ca.* 850 °C, Ni-catalyst) [4, 5]. This two-step process incurs high energy and capital demands. Key barriers to CO$_2$ hydrogenation replacing/supplementing this industry include catalyst stability and methanol yields. Another key consideration is reaction selectivity, as side reactions yield CO, CH$_4$ and C$_2$–C$_4$ hydrocarbons which incur significant downstream separation costs. Additionally, methanol synthesis through direct CO$_2$ hydrogenation with H$_2$ is restricted by thermodynamic equilibria; hydrogenation to methanol is dominant at low reaction temperatures or high reaction pressure. Catalyst design is therefore vital, with a "good" catalyst for CO$_2$ hydrogenation required to show strong adsorption and transportation of CO$_2$, high concentration of hydrogenation sites, ability to stabilise intermediates and resistance towards water-induced deactivation. Cu has been extensively studied for CO$_2$ hydrogenation, however it is often associated with
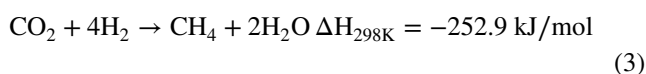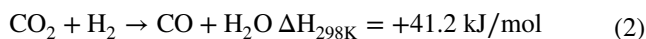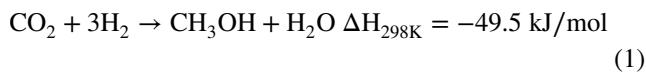
✉ Hasliza Bahruji
  bahrujih@cardiff.ac.uk

1 School of Chemistry, Cardiff Catalysis Institute, Cardiff University, Main Building, Park Place, Cardiff CF10 3AT, UK

2 The UK Catalysis Hub, Research Complex at Harwell, Harwell, Oxon OX11 0FA, UK

deactivation on-stream [6]. This arises as catalytic activity is highly dependent on copper surface area whilst water, which is formed through the reverse water gas shift reaction, induces sintering of copper nanoparticles [7–9]. In contrast Pd, a well-known hydrogenation catalyst, is known to be stable towards water-induced sintering [10]. We previously reported Pd/ZnO to be an active catalyst for CO_2 hydrogenation, with the choice of catalyst preparation method and Pd precursor shown to impact significantly upon product selectivity [11]. Investigation into the structural properties of Pd and PdZn species is key to understanding the origin of this catalytic activity, which will inform the designing of more methanol-selective catalysts. ZrO_2-supported In_2O_3 showed high activity and 100% methanol selectivity, with this behaviour attributed to rapid formation and annihilation of oxygen vacancies during CO_2 hydrogenation [12].

C=O dissociation has been identified as the rate determining step in CO_2 hydrogenation, requiring 2.97 eV in the gas phase [13]. The catalytic reaction proceeds first through hydrogenation of CO_2 to a formate intermediate [14], which then undergoes C–O bond dissociation and hydrogenation to form methoxide species [15]. Meanwhile, CO_2 methanation requires two consecutive C–O bond dissociation events to yield carbon, which undergoes hydrogenation to form methane [13].

$$CO_2 + 3H_2 \rightarrow CH_3OH + H_2O \quad \Delta H_{298K} = -49.5 \text{ kJ/mol} \tag{1}$$

$$CO_2 + H_2 \rightarrow CO + H_2O \quad \Delta H_{298K} = +41.2 \text{ kJ/mol} \tag{2}$$

$$CO_2 + 4H_2 \rightarrow CH_4 + 2H_2O \quad \Delta H_{298K} = -252.9 \text{ kJ/mol} \tag{3}$$

In this study we prepared $PdZn/TiO_2$ catalysts via solvent free chemical vapour impregnation (CVI) method to avoid surface contamination that can occur from the use of solvents. The influence of PdZn morphologies on the activity towards CO_2 hydrogenation are reported. This will be achieved through studying the effect that reductive heat treatment conditions have upon physico-chemical properties of catalysts and their CH_4, CO and CH_3OH productivities.

2 Experimental

All supported catalysts were prepared via CVI. The procedure for preparing 2 g of 5% $PdZn/TiO_2$ (1Pd:5Zn molar ratio) is as follows; $Pd(acac)_2$ (0.29 g, 0.939 mmol) and $Zn(acac)_2$ (1.23 g, 4.698 mmol) were physically mixed with TiO_2 (P25, 1.58 g, Sigma Aldrich) for 1 min. The dry mixture was transferred to a 50 ml Schlenk flask and then evacuated at room temperature (*ca*. 10^{-3} bar). Following this, the mixture was gradually heated to 145 °C. After 1 h the resulting pre-catalyst was recovered, prior to

calcination in static air (500 °C, 16 h, 10 °C). All catalysts were reduced ex situ in a flow of 5% H_2/Ar prior to assessment (at 400, 500 or 650 °C). For 7% $PdZn/TiO_2$ and 10% $PdZn/TiO_2$, a similar procedure was followed; increasing the wt% of Pd while a Pd: Zn molar ratio of 1:5. This method is referred as co-CVI.

Two sets of catalysts $^2Pd–^1Zn–TiO_2$ and $^2Zn–^1Pd–TiO_2$ were also prepared using sequential CVI. For $^2Pd–^1Zn–TiO_2$, $Zn–TiO_2$ was first prepared as follows; $Zn(acac)_2$ (1.23 g, 4.698 mmol) was physically mixed with TiO_2 (P25, 1.58 g, Sigma Aldrich) for 1 min then was transferred to a 50 ml Schlenk flask. The mixture was then evacuated at room temperature (*ca*. 10^{-3} bar) and gradually heated to 145 °C. The system was then heated at this temperature for 1 h, after which it was allowed to cool to room temperature. $Pd(acac)_2$ (0.29 g, 0.939 mmol) was then physically mixed with the $Zn–TiO_2$ for 1 min. The resulting mixture was evacuated again at room temperature (*ca*. 10^{-3} bar) and gradually heated to 145 °C. After 1 h the resulting pre-catalyst was recovered, prior to calcination in static air (500 °C, 16 h, 10 °C). A similar procedure was repeated in preparing $^2Zn–^1Pd–TiO_2$, though Pd was added first, followed by Zn. All catalysts were reduced in situ at 400 °C in H_2 (30 ml min^{-1}, 1 h) unless stated otherwise.

Catalysts were characterised using a range of techniques. Powder X-ray diffraction (XRD) patterns were obtained at room temperature using an Enraf Nonus FR590 diffractometer fitted with a hemispherical analyser, using Cu Kα radiation (l 1/4 1.54 A). X-ray photoelectron spectra (XPS) were recorded on a Kratos Axis Ultra-DLD XPS spectrometer with a monochromatic Al Kα source (75–150 W) and analyser pass energies of 160 eV (for survey scans) or 40 eV (for detailed scans). Samples were mounted using a double-sided adhesive tape and binding energies referenced to the C (1s) binding energy of adventitious carbon contamination which was taken to be 284.7 eV. Data were analysed using Casa XPS software. To provide detailed morphological and compositional information at micro and nano-scales, samples were analysed on a JEOL 2100 (LaB6) high-resolution transmission electron microscope (HRTEM) system fitted with a high-resolution Gatan digital camera (2 k 2k) and a dark held HAADF/Z-contrast detector. Samples were suspended in DI water and *ca*. 1 μl was added to the TEM grid and dried. Lattice d-spacings were determined using Digital Micrograph software. Surface area analysis was performed on a Nova 2200e Quantachrome. The catalyst was pre-treated under vacuum at 250 C for 2 h before the surface area was determined by 5 point N_2 adsorption at − 196 °C and the data was analysed using the BET method. Diffuse Reflectance Infrared Fourier Transform Spectroscopy (DRIFTS) spectra were collected on a Bruker Tensor 27 spectrometer fitted with a liquid N_2-cooled MCT detector. Samples were housed in a Praying Mantis high temperature

diffuse reflection environmental reaction chamber (HVC-DRP-4) fitted with zinc selenide windows.

Catalytic assessment for CO_2 hydrogenation was carried out in a custom built fixed-bed continuous-flow reactor. The pelleted catalyst (0.5 g, 425–500 μm) was placed in a stainless tube reactor with internal diameter of 0.5 cm and length 50 cm, occupying a length of *ca*. 10 cm. Prior to testing, catalysts were pre-reduced in situ in a flow of H_2 gas (30 ml min^{-1}, 1 atm, 400 °C, 1 h) and subsequently cooled to room temperature. The system was then pressurised to 20 bar with the reactant gas (1 CO_2: 3 H_2: 1 N_2 molar ratios), heated to 250 °C and reaction was carried out for 4 h. A standard reaction gas flow rate of 30 ml min^{-1} was used throughout (GHSV *ca*. 916 h^{-1}). To avoid product condensation, post-reactor lines and valves were heated at 130 °C. Products were analysed via on-line gas chromatography using an Agilent 7890 system fitted with both FID and TCD detectors. Nitrogen was used as an internal standard. The reaction was carried out for 4 h.

3 Results and Discussion

## 3.1 Catalyst Characterisation

3.1.1 XRD Analysis

XRD was used as a primary technique to confirm formation of the crystalline PdZn phase on TiO_2. However, the (111) and (200) β-PdZn alloy reflections (at 41.2° and 44.1° respectively) [16] overlap with the (111) and (210) planes for rutile TiO_2. This led to difficulty in detecting the PdZn

alloy. Indeed, formation of this alloy can only be definitively identified in the XRD of the 5% $PdZn/TiO_2$ which had been reduced for 1 h at 650 °C (Fig. 1). The broadening and increasing intensity of the reflections at 40.9° and 44.0° in comparison to the P25 TiO_2 support implies formation of the PdZn alloy. Following reduction at 650 °C the PdZn alloy was clearly observed at 40.9° and 44.0°. Diffractions corresponding to a $ZnTiO_3$ phase were also observed in Fig. 1 following reduction at 650 °C. Accompanied by a disappearance of the ZnO reflection at 31.6°, this suggests that incorporation of ZnO into the TiO_2 lattice occurs during reduction at 650 °C.

To confirm whether high temperature reduction does indeed lead to a phase change, N_2 physisorption studies were carried out. It is clear from Table 1 that the impregnation of $Pd(acac)_2$ and $Zn(acac)_2$ does not lead to a significant decrease in catalyst surface area, relative to unmodified TiO_2 (P25) (Table 1, Entry 1). A gradual decrease in BET surface area is observed upon increasing the reduction temperature from 400 to 650 °C (Table 1, Entries 3 and 5). This can be attributed to TiO_2 undergoing partial conversion from anatase to the rutile phase. Additionally, the formation of the $ZnTiO_3$ phase also contributes to the reduction of the surface area [17]. From the XRD it can be seen that the ZnO phase disappears upon heating to 650 °C.

X-ray diffractograms of 7% $PdZn/TiO_2$ and 10% $PdZn/TiO_2$ shown in Fig. 2. Whilst similar to that of 5% $PdZn/TiO_2$, the PdZn (111) peak at 40.78° is more pronounced for 7% $PdZn/TiO_2$ than either 5 or 10% wt loading catalysts. Figure 2 also shows the diffraction patterns of the catalyst prepared via sequential CVI, $^2Pd–^1Zn–TiO_2$ and $^2Zn–^1Pd–TiO_2$. These samples showed relatively pronounced

Fig. 1 XRD of P25 and PdZn/TiO₂ catalyst after hydrogen reduction at 400, 550 and 650 °C
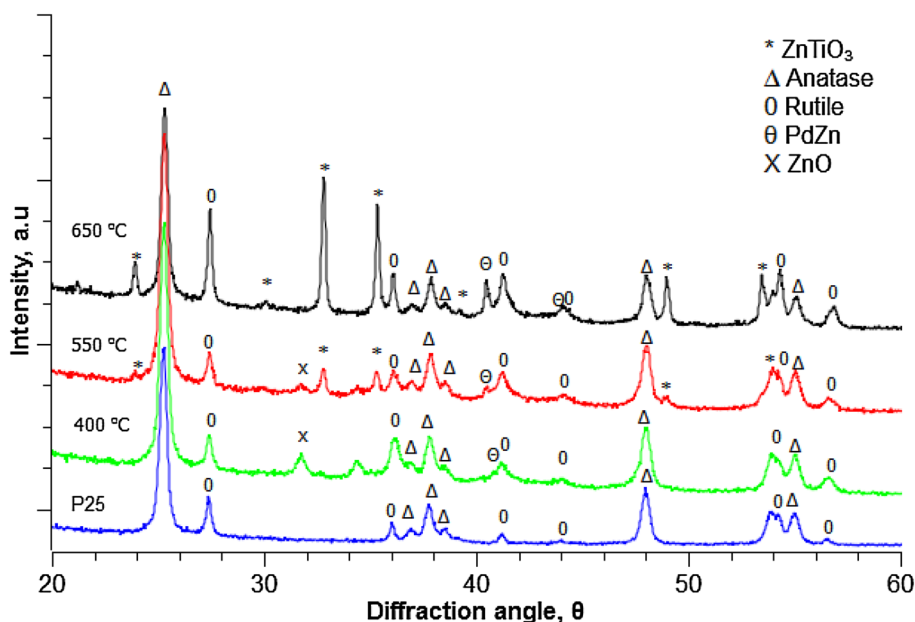
Table 1 The effect of reductive heat treatment conditions on the physico- chemical properties of 5% PdZn/TiO$_2$

Entry	Reduction conditions[a]	PdZn size (nm)[b]	BET surface area (m^2 g^{-1})[c]	B.E PdO (eV)[d]	B.E PdZn (eV)[d]	B.E Pd (eV)[d]
1	Unmodified TiO$_2$	–	50	–	–	–
2	n/a	4.1[e]	43	336.6	–	–
3	5% H$_2$/Ar, 400 °C, 1 h	3.9	44	–	335.8	335.0
4	5% H$_2$/Ar, 550 °C, 1 h	4.4	39	–	336.1	335.0
5	5% H$_2$/Ar, 650 °C, 1 h	5.6	38	–	336.1	335.0

[a]All catalysts were pre-calcined (500 °C, 10 °C min^{-1}, 16 h)

[b]Determined by TEM

[c]Determined by N$_2$ physisorption

[d]Determined by XPS

[e]PdO particle size

Fig. 2 XRD analysis of 7 and 10 wt% PdZn/TiO$_2$ catalysts; and catalysts prepared via sequential CVI, ^{2}Pd–^{1}Zn–TiO$_2$ and ^{2}Zn–^{1}Pd–TiO$_2$ after hydrogen reduction at 400 °C
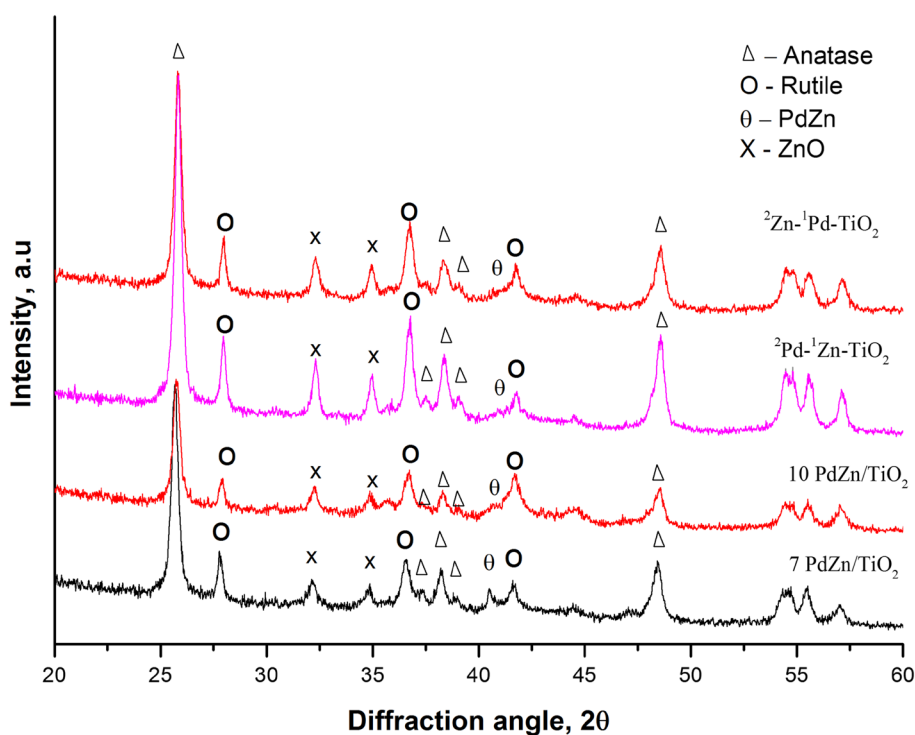

ZnO peaks (32.31° and 34.96°) when compared with 5% PdZn/TiO$_2$ prepared by co-CVI method. ZnO crystallite size was determined using the Scherrer equation and ZnO peak at 32.31°. In this way ^{2}Zn–^{1}Pd–TiO$_2$ showed a ZnO crystallite size of 40.6 nm and ^{2}Pd–^{1}Zn–TiO$_2$ 31.3 nm. These values are significantly higher than the 29.0 nm determined for the analogous co-CVI catalyst.

3.1.2 XPS Analysis

The synthesised CVI catalysts were calcined in static air (500 °C, 16 h) to ensure complete removal of acetylacetonate precursors. XPS analysis of the calcined catalyst is shown in Fig. 3a. The Pd 3d, O 1s and Zn LMM Auger electron peak positions were calibrated using the C 1s signal at 284.8 eV. Transformation of Pd to the PdZn alloy can be observed in the Pd 3d signal. Following calcination at 500 (Fig. 3a), the peak is at 336.5 eV, which corresponds to oxidised Pd^{2+} in PdO. Following annealing in H$_2$ (400 °C, 1 h) the peak shifts towards a lower binding energy of 335 eV and the appearance of a shoulder at 336 eV. The observed shift in binding energy occurs due to a change in the Pd environment, which depends on the localised charge on the emitting atom [18]. Indeed, a shift towards lower binding energies indicates a decrease in electronic charge, resulting from decreased electronegativity of adjacent substituents. This implies that the

Fig. 3 Pd 3d, Zn LMM Auger electron and O 1s XPS analysis of 5% PdZn/TiO$_2$ following **a** calcination at 500 °C and subsequent reduction in H$_2$ at **b** 400 °C and **c** 650 °C
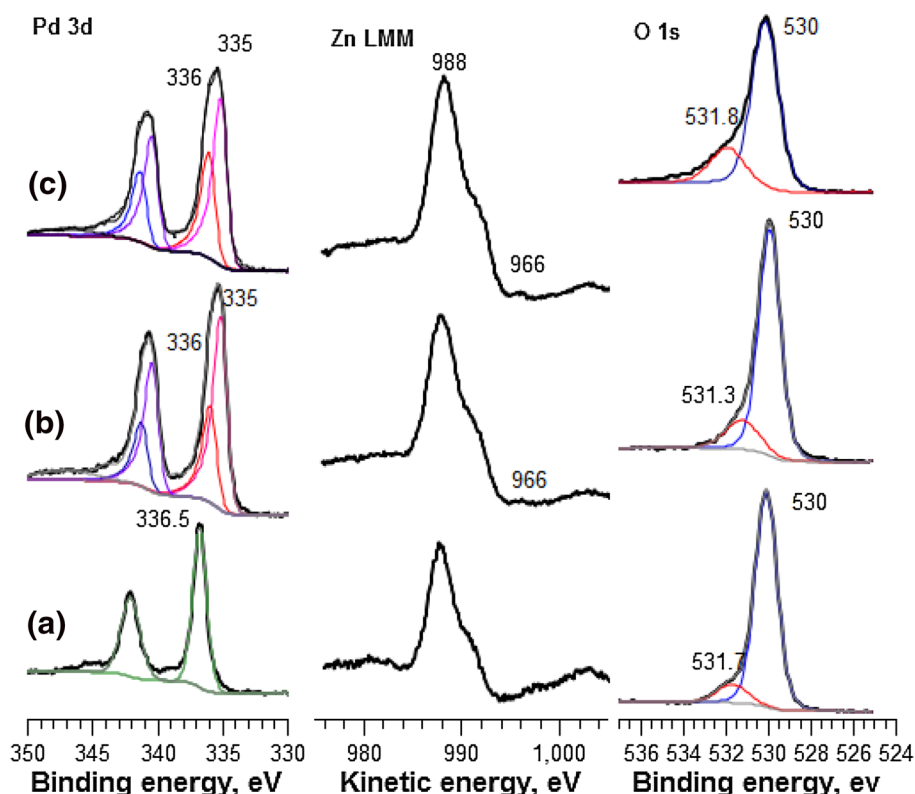
asymmetric peak at 335 eV corresponds to Pd$^{\circ}$. Meanwhile, electronic changes occur in Pd due to the intermetallic bond with Zn upon forming PdZn, thereby effecting changes in the Pd localised charge. A correlation between the shoulder at 336 eV and formation of the PdZn alloy is apparent following reduction at 400 and 650 °C. PdZn alloy formation can be further established through close observation of the Zn LMM Auger electron region. The calcined catalyst shows a peak at K.E = 988 eV, which corresponds to ZnO. Meanwhile, a shoulder at 991 eV is often indicative of interstitial Zn on the catalyst surface. When reduced at 400 and 650 °C, a small peak appeared at 966 eV. This is similar to the Auger electronic position of Zn alloy [19, 20]. It is small because the oxide component is dominant formation of the Pd:Zn 1:1 alloy will only use 20% of the available Zn and also surface Zn metal may well oxidise on exposure to air.

Following calcination, the O 1s spectra showed two peaks at 530 and 531.7 eV. These represent two chemically distinct oxygen environments. The principal peak at 530 eV, is due to lattice oxygen and most likely originates from TiO$_2$. The contribution at 531.7 eV can be attributed to chemisorbed oxygen, which can form through adsorption of water at surface oxygen vacancies [21, 22]. Reduction at 400 or 650 °C led the peak shoulder to increase in intensity. This is indicative of an increased concentration of surface defects, and suggests that these catalysts contain increased oxygen deficiency at the surface. XRD analysis confirms reaction of

ZnO with TiO$_2$ lattice to form a crystalline ZnTiO$_3$ phase. Such a change has been reported to induce surface defects on TiO$_2$ [23]. This is consistent with the appearance of chemisorbed oxygen at 531.7 eV, in the O 1s XPS spectrum [24].

Figure 4a shows the Pd 3d regions in XPS spectra for PdZn/TiO$_2$ at 7 and 10 wt% loadings. The catalysts were reduced prior to XPS analysis (H$_2$, 400 °C, 1 h) to promote PdZn formation. Peaks corresponding to Pd$^{\circ}$ (335 eV) and PdZn alloy (336 eV) were observed for both catalysts. However, based on the curve-fitted peak of Pd 3d signals, 7% PdZn/TiO$_2$ showed a relatively high PdZn alloy: Pd$^{\circ}$ ratio. Figure 4b shows the Pd 3d region in XPS spectra for ^{2}Pd–^{1}Zn–TiO$_2$ and ^{2}Zn–^{1}Pd–TiO$_2$. In addition to PdZn (335 eV) and Pd$^{\circ}$ (336 eV) a peak at 337 eV, corresponding with PdO was observed.

3.1.3 CO Adsorption Studies

CO was used as a probe molecule to compare the surface adsorption properties of PdZn/TiO$_2$ catalysts. Spectra are shown in Fig. 5. Following reduction at 150 °C (1 h), the DRIFTS spectrum of PdZn/TiO$_2$ shows a band at 2075 cm^{-1}, which corresponds to linearly adsorbed CO. Bands at 1985 and 1922 cm^{-1} are attributed to bridging CO species; at corner and edge sites respectively [25]. Bands associated with bridging CO are relatively intense when compared with the band a 2075 cm^{-1}, suggesting that the catalyst surface

Fig. 4 Pd 3d, XPS analysis of **a** 7% PdZn/TiO$_2$ and 10% PdZn/TiO$_2$ following reduction in H$_2$ at 400 °C and **b** catalysts prepared via sequential CVI, ^{2}Pd–^{1}Zn–TiO$_2$ and ^{2}Zn–^{1}Pd–TiO$_2$ after hydrogen reduction at 400 °C
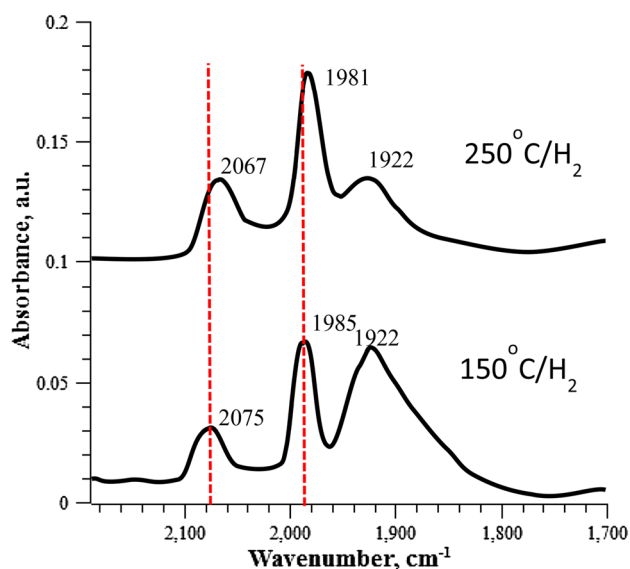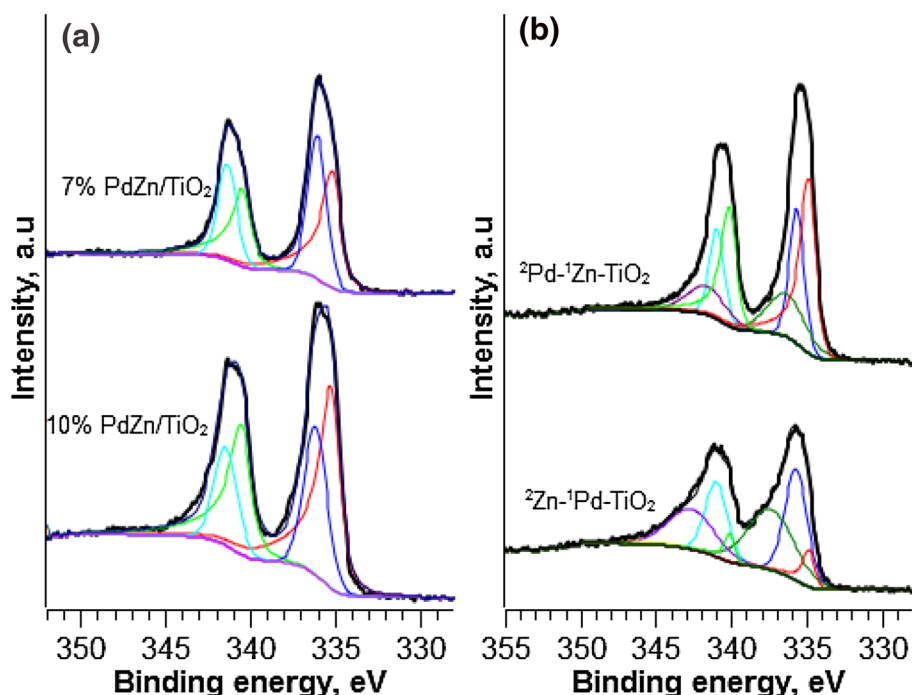
Fig. 5 CO DRIFTS spectra of 5% PdZn/TiO$_2$ following reduction at 150 and 250 °C

consists mainly of metallic Pd. When reduced at 250 °C (1 h) a significant change in the CO feature is observed. In particular, the broad band at *ca*. 1922 cm^{-1}, associated with bridging CO at edge sites, becomes less intense. These results suggest that reduction of the catalyst in hydrogen promotes formation of the PdZn alloy, as evidenced by disappearance of the bridging CO band at *ca*. 1922 cm^{-1}. However, the surface is consists of Pd, which suggests the presence of isolated Pd species which require higher temperatures to alloy with Zn [26].

3.1.4 Surface and Morphological Analyses

Morphological changes, ie the size and shape of nanoparticles within 5% PdZn/TiO$_2$ following high temperature reductions (at 400, 550 and 650 °C) were studied via TEM analysis (Fig. 6). Representative micrographs and particle size distributions are shown in Fig. 3, with mean particle sizes summarised in Table 1. It is clear from Fig. 1a that CVI produced nanoparticles of *ca*. 4.1 nm average size, which are well dispersed on the TiO$_2$ support. Reductive treatment at 400 °C led to a contraction in particle size (Fig. 3b, 3.9 nm). Further increase in reduction temperature, to 550 or 650 °C, led to particle growth (4.4 and 5.6 nm respectively). High resolution TEM analysis following reduction at 400 °C, reveals a d-spacing of 0.21 nm on some metal particles, which corresponds to the PdZn (111) lattice plane of PdZn nanoparticles [27, 28]. TEM analysis of 7 and 10 wt% PdZn/TiO$_2$ shows that CVI affords evenly distributed PdZn nanoparticles across the surface of TiO$_2$ (Fig. 7). Furthermore, particle size analysis shows the mean particle size to increase with metal loading, from 5.3 nm ($\pm$ 2.3 nm) at 7 wt% PdZn to 5.5 nm ($\pm$ 1.9 nm) for 10 wt% PdZn on TiO$_2$.

3.2 Catalytic Activity

Characterisation studies showed a general increase in PdZn nanoparticle size upon increasing reductive heat treatment

temperature from 400 to 650 °C. A corresponding decrease in BET surface area was attributed to an increasing degree of transformation to rutile TiO_2 and $ZnTiO_3$ phases. To determine whether CO_2 hydrogenation on PdZn is structure-sensitive, these catalysts were assessed under standard reaction conditions (P = 20 bar, 1 CO_2: 3 H_2: 1 N_2, 30 ml min^{-1},

250 °C). The results in Table 2 show no defined correlation between reduction temperature and CO_2 conversion. Indeed, the samples reduced at 400, 550 and 650 °C afforded 10.1, 10.5 and 9.1% conversion respectively (Table 2, Entries 1 and 3). Across this range however, an appreciable increase in methanol productivity was observed, reaching 1710 mmol
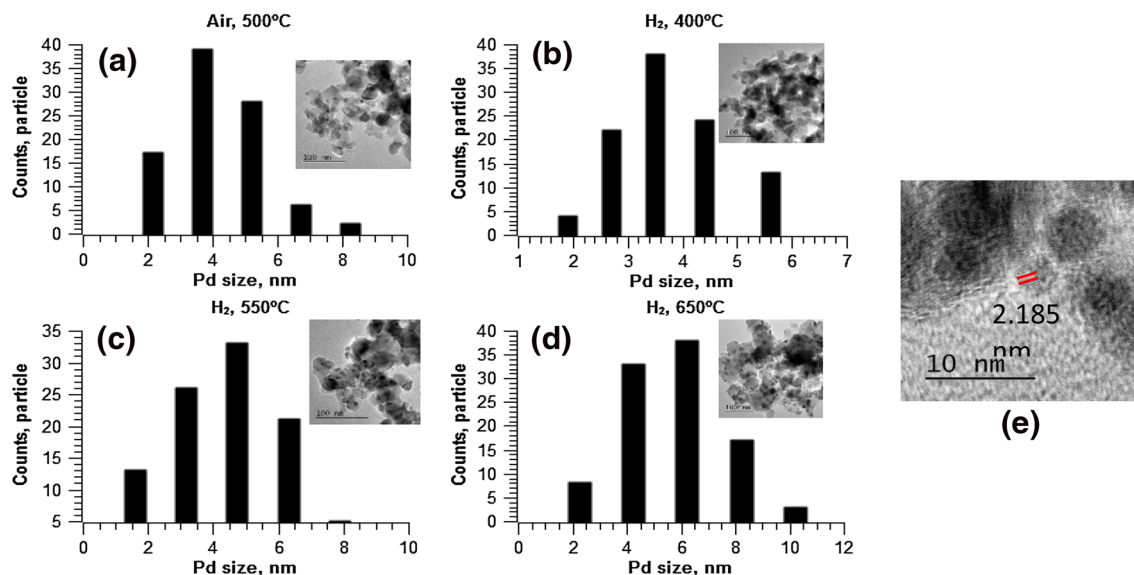
Fig. 6 TEM images and particle size distribution histograms for 5% PdZn/TiO$_2$ following; **a** calcination at 500 °C and subsequent reduction in H$_2$ at **b** 400 °C, **c** 550 °C and **d** 650 °C. **e** A HR-TEM image of PdZn nanoparticles in 5% PdZn/TiO$_2$ following reduction at 400 °C, showing a *d*-spacing calculation
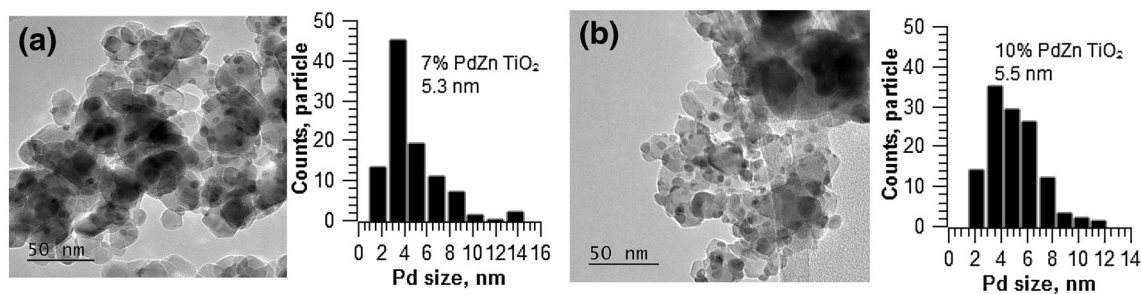
Fig. 7 TEM images and particle size distribution of 7% PdZn/TiO$_2$ and 10% PdZn/TiO$_2$ after reduction at 400 °C

Table 2 The effect of reduction temperature on catalytic activity

Entry	Reduction temperature (°C)	χ CO$_2$ (%)	S (CH$_3$OH) (%)	S (CO) (%)	S (CH$_4$) (%)	mmol (CH$_3$OH) (kg$_{cat}^{-1}$ h^{-1})	mmol (CO) (kg$_{cat}^{-1}$ h^{-1})	mmol (CH$_4$) (kg$_{cat}^{-1}$ h^{-1})
1	400	10.1	40	59	0.1	1420	1550	8
2	550	10.5	35	64	0.05	1190	2170	3
3	650	9.1	58	41	0	1710	1210	0

Catalytic data at 4 h of reaction

All catalysts were pre-calcined (500 °C, 10 °C min^{-1}, 16 h)

kg_{cat}^{-1} h^{-1} (58.6% selectivity, 5.3% yield) when the catalyst was treated at 650 °C. Another key observation is the relationship between reduction temperature and CO_2 methanation rates, with CH_4 productivity being immeasurable when the catalyst was reduced at 650 °C. In industrial methanol synthesis processes, CH_4 formation incurs significant downstream separation costs. Metallic Pd is a well-known methanation catalyst and this is likely to occur at the Pd-metal oxide interface [13, 29]. It is clear from data in Table 2 that PdZn alloy formation significantly inhibits methane formation, thereby suggesting a high degree of PdZn alloying. When reduced at 400 °C, the catalyst has some limited activity for CO_2 methanation, with a CH_4 productivity of 8 mmol kg_{cat}^{-1} h^{-1} (*ca.* 0.1% selectivity). This suggests the presence of non-alloyed Pd species, for example isolated Pd°. For commercial applications, even 0.1% CH_4 selectivity would prove problematic and expensive [30, 31]. Complete suppression of CH_4 formation can be achieved through reduction at 650 °C as shown in Table 2 Entry 3 (note; the GC-FID detection limit for CH_4 was 1 ppm or ~0.0005% effective yield). Studies summarised in Tables 1 and 2 do not show a definitive correlation between reduction temperature, physico-chemical properties (BET surface area, PdZn particle size) and catalyst performance. However, XPS analysis did show a shift in the position of the PdZn peak towards higher binding energies with increasing reduction temperature, suggesting a high degree of alloying with Zn. Meanwhile XRD analysis showed incorporation of ZnO into the TiO_2 following reduction at 650 °C, leading to formation of a $ZnTiO_3$ phase. Given the relatively high methanol productivity shown by $PdZn/TiO_2$ following reduction at 650 °C, we therefore suggest that the presence of $ZnTiO_3$ promotes CO_2 hydrogenation through increasing the number of available surface oxygen vacancies.

To further study whether the structure of PdZn nanoparticles has a significant effect upon catalyst activity, 5% PdZn/TiO_2 was prepared by CVI with Pd and Zn impregnated onto TiO_2 in either one (co-CVI) or two (sequential) steps. The co-CVI catalyst was prepared as detailed in the experimental. Meanwhile for sequential CVI catalysts monometallic Pd/TiO_2 and Zn/TiO_2 were first prepared, followed by impregnation of the second metal, calcination in static air

(500 °C, 16 h) and in situ reduction (400 °C, 1 h, 30 ml min^{-1} H$_2$).The performance of these catalysts is summarised in Table 3. CO_2 conversion showed a strong dependence on the preparation method. Co-impregnation of Pd and Zn (Table 3, Entry 3) led to a higher CO_2 conversion and methanol productivity than when metals were impregnated sequentially (Table 3, Entries 1 and 2).

Sequential addition of Pd to Zn/TiO_2 (^{2}Pd–^{1}Zn–TiO_2) affords 8.6% CO_2 conversion, whilst the inverse ^{2}Zn–^{1}Pd–TiO_2 catalyst shows notably lower CO_2 conversion of 6.7%. XPS analysis (Fig. 4b) showed the presence of PdO on the surface and XRD (Fig. 2) revealed larger ZnO crystallites for catalysts prepared via sequential CVI. This suggests that co-addition of Pd and Zn affords a higher degree of Pd–Zn alloying. It is difficult to assign formation of the PdZn alloy to specific differences between these synthesis methods (Table 3, Entry 3), but is likely that there is an interaction between Pd(acac)$_2$ and Zn(acac)$_2$ precursors. This might promote formation of the PdZn active site. Unfortunately, due to the instability of acetylacetonate precursors, it was not possible to study such interactions spectroscopically.

Another approach to increase methanol yields would be to increase the concentration of active sites on the TiO_2 support. PdZn alloy nanoparticles have previously been reported as both the active site and a stabiliser of formate intermediates [11, 32]. With an aim to increase the number of PdZn sites the Pd loading was increased to 7 and 10 wt%. Across this range, the Pd: Zn molar ratio was maintained at 1:5 as this was previously reported to afford optimal methanol yields [32]. Data in Table 4 summarises the performance of these catalysts; CO_2 conversion and product selectivities, at temperatures of between 190 and 250 °C.

7 wt% PdZn/TiO_2 and 5 wt% PdZn/TiO_2 showed comparable CO_2 conversion at a reaction temperature of 250 °C (*ca.* 10%). Further increasing the Pd loading to 10 wt% resulted in a decrease in catalytic activity at high temperatures, with CO_2 conversion of 5.7%. It is likely that the maximum loading of well-dispersed metal, achievable in CVI, is restricted such that high dispersion is dependent on close proximity between acetylacetonate precursor and support. TEM analysis shows the mean PdZn particle size

Table 3 Catalytic activity of 5% PdZn/TiO_2 catalysts prepared by CVI with metals impregnated either sequentially or simultaneously

Entry	Catalyst[a]	χ CO_2 (%)	S (CH_3OH) (%)	S (CO) (%)	S (CH_4) (%)	mmol (CH_3OH) kg_{cat}^{-1} h^{-1}	mmol (CO) (kg_{cat}^{-1} h^{-1})	mmol (CH_4) (kg_{cat}^{-1} h^{-1})
1	^{2}Pd–^{1}Zn–TiO_2	8.6	39	60	0.2	1070	1670	5.8
2	^{2}Zn–^{1}Pd–TiO_2	6.7	11	88	0.2	247	1910	4.5
3	PdZn/TiO_2	10.1	40	59	0.1	1420	1550	8

[a]All catalysts were pre- calcined (500 °C, 10 °C min^{-1}, 16 h) and reduced in situ (400 °C, H$_2$, 1 h) prior to reaction, ^{1} and ^{2} denote the order of sequential metal impregnations

Table 4 The catalytic activity of 5 wt% PdZn/TiO$_2$, 7 wt% PdZn/TiO$_2$ and 10 wt% PdZn/TiO$_2$ (Pd: Zn = 1: 5 molar) at different reaction temperatures

Entry	Catalyst[a]	T (°C)[b]	χCO$_2$ (%)	S (CH$_3$OH) (%)	S (CO) (%)	mmol (CH$_3$OH) (kg$_{cat}^{-1}$ h^{-1})	mmol (CO) (kg$_{cat}^{-1}$ h^{-1})
1	5% PdZn(1:5)/TiO$_2$	190	1.5	97	2	592	17.8
		210	2.5	59	40	606	411
		230	5.7	46	53	1090	1250
		250	10.1	40	59	1420	1550
2	7% PdZn(1:5)/TiO$_2$	190	3.5	99	1.0	1110	11
		210	5.3	90	9	1560	162
		230	7.1	79	20	1810	473
		250	10.3	61	38	2040	1280
3	10% PdZn(1:5)/TiO$_2$	190	3.8	66	33	823	423
		210	4.2	78	22	855	252
		230	4.9	60	39	961	630
		250	5.7	23	77	426	1430

[a]All catalysts were pre- calcined (500 °C, 10 °C min^{-1}, 16 h) and followed by reduction (400 °C, H$_2$, 1 h)

[b]Reaction temperature. Catalytic data at 4 h of reaction

to increase with increasing loading. It likely that the low activity observed for the 10 wt% PdZn catalyst stems from poor distribution of the acetylacetonates across the support surface. Furthermore, at such high loadings, it is possible that calcination for 16 h (at 500 °C) was not sufficient to remove all carbon species. Residual carbon contaminants on the catalyst surface would be expected to have a detrimental effect upon catalytic activity [32].

The effect of varying reaction temperature on the performance of these catalysts is shown in Table 4. A general trend towards higher conversion was observed with increasing reaction temperature. For example, conversion over 5% PdZn/TiO$_2$ increased from 1.5 to 10.1% moving from 190 to 250 °C. This was associated with increased methanol productivities, from 592 mmol kg$_{cat}^{-1}$ h^{-1} to 1420 mmol kg$_{cat}^{-1}$ h^{-1}. However, high temperatures do not make CO$_2$ hydrogenation more kinetically favourable, as CO$_2$ methanation and reverse water gas shift reactions become more favourable and consequently affect methanol selectivity. It is interesting that although 5 and 7 wt% catalysts comparable CO$_2$ conversion at 250 °C, activities at lower reaction temperatures differ greatly. At 190 °C, the lowest reaction temperature at which the 7 wt% catalyst was able to initiate CO$_2$ conversion, 3.5% CO$_2$ conversion and 97% methanol selectivity were observed (1110 mmol (CH$_3$OH) kg$_{cat}^{-1}$ h^{-1}). The 7 wt% catalyst also showed superior activity to 5 wt% at both 210 and 230 °C. We consider this to be an important observation as it suggests that the catalytic hydrogenation of CO$_2$ to methanol is likely to be restricted by thermodynamic equilibria at higher reaction temperatures. However, at temperatures of below 250 °C, where the reaction is kinetically as opposed to thermodynamically limited, an increase in the

concentration of active sites significantly improves methanol productivity.

4 Conclusions

CVI is an effective method for preparing highly dispersed, alloyed PdZn nanoparticles with mean diameters in the region of 3–6 nm. Reductive heat treatment of these catalysts leads to improved methanol productivities and has been shown to significantly inhibit undesirable methane formation reactions. Spectroscopic studies show that when reduced at a temperature of 650 °C, a ZnTiO$_3$ phase forms, which correlates with an increase in methanol yield. Preparation of PdZn/TiO$_2$ catalysts whereby Pd and Zn were added sequentially, highlights the importance of interaction between Pd(acac)$_2$ and Zn(acac)$_2$ in forming the PdZn alloy active site, with inactive PdO and ZnO phases forming during these preparations. These catalysts were, in turn, less active than co-CVI analogues, further showing the role of the PdZn alloy in catalysing CO$_2$ hydrogenation. Future studies will probe the role that metal acetylacetone-metal acetylacetonate interactions play in formation of the desired PdZn alloy.

References

1. Rockstrom J, Steffen W, Noone K, Persson A, Chapin FS, Lambin EF, Lenton TM, Scheffer M, Folke C, Schellnhuber HJ, Nykvist B, de Wit CA, Hughes T, van der Leeuw S, Rodhe H, Sorlin S, Snyder PK, Costanza R, Svedin U, Falkenmark M, Karlberg L, Corell RW, Fabry VJ, Hansen J, Walker B, Liverman D, Richardson K, Crutzen P, Foley JA (2009) A safe operating space for humanity. Nature 461:472–475
2. Olah GA (2005) Beyond oil and gas: the methanol economy. Angew Chem Int Ed 44:2636–2639
3. Schlögl R (2010) The role of chemistry in the energy challenge. ChemSusChem 3:209–222
4. Behrens M (2014) Heterogeneous catalysis of CO_2 conversion to methanol on copper surfaces. Angew Chem Int Ed 53:12022–12024
5. Aresta M, Dibenedetto A (2007) Utilisation of CO_2 as a chemical feedstock: opportunities and challenges. Dalton Trans 28:2975–2992
6. Prieto G, Zečević J, Friedrich H, de Jong KP, de Jongh PE (2013) Towards stable catalysts by controlling collective properties of supported metal nanoparticles. Nat Mater 12:34–39
7. Kasatkin I, Kurr P, Kniep B, Trunschke A, Schlögl R (2007) Role of lattice strain and defects in copper particles on the activity of $Cu/ZnO/Al_2O_3$ catalysts for methanol synthesis. Angew Chem 119:7465–7468
8. Sun JT, Metcalfe IS, Sahibzada M (1999) Deactivation of $Cu/ZnO/Al_2O_3$ methanol synthesis catalyst by sintering. Ind Eng Chem Res 38:3868–3872
9. Wu J, Saito M, Takeuchi M, Watanabe T (2001) The stability of Cu/ZnO-based catalysts in methanol synthesis from a CO2-rich feed and from a CO-rich feed. Appl Catal A 218:235–240
10. Conant T, Karim AM, Lebarbier V, Wang Y, Girgsdies F, Schlögl R, Datye A (2008) Stability of bimetallic Pd–Zn catalysts for the steam reforming of methanol. J Catal 257:64–70
11. Bahruji H, Bowker M, Hutchings G, Dimitratos N, Wells P, Gibson E, Jones W, Brookes C, Morgan D, Lalev G (2016) Pd/ZnO catalysts for direct CO_2 hydrogenation to methanol. J Catal 343:133–146
12. Martin O, Martín AJ, Mondelli C, Mitchell S, Segawa TF, Hauert R, Drouilly C, Curulla-Ferré D, Pérez-Ramírez J (2016) Indium oxide as a superior catalyst for methanol synthesis by CO_2 hydrogenation. Angew Chem Int Ed 55:6261–6265
13. Wei W, Jinlong G (2011) Methanation of carbon dioxide: an overview. Front Chem Sci Eng 5:2–10
14. Kim Y, Trung TSB, Yang S, Kim S, Lee H (2016) Mechanism of the surface hydrogen induced conversion of CO_2 to methanol at Cu(111) step sites. ACS Catal 6:1037–1044
15. Fisher IA, Bell AT (1997) In-situ infrared study of methanol synthesis from H_2/CO_2 over Cu/SiO_2 and $Cu/ZrO_2/SiO_2$. J Catal 172:222–237
16. Tew MW, Emerich H, van Bokhoven JA (2011) Formation and characterization of PdZn alloy: a very selective catalyst for alkyne semihydrogenation. J Phys Chem C 115:8457–8465
17. Arin J, Thongtem S, Phuruangrat A, Thongtem T (2017) Characterization of ZnO–TiO_2 and zinc titanate nanoparticles synthesized by hydrothermal process. Res Chem Intermed 43:3183–3195
18. van der Heide P (2011) Atoms, ions, and their electronic structure. In: X-ray photoelectron spectroscopy. Wiley, New York, pp 13–26
19. Cocco F, Elsener B, Fantauzzi M, Atzei D, Rossi A (2016) Nano-sized surface films on brass alloys by XPS and XAES. RSC Advances 6:31277–31289
20. Moffitt CE, Wieliczka DM, Yasuda HK (2001) An XPS study of the elemental enrichment on aluminum alloy surfaces from chemical cleaning. Surf Coat Technol 137:188–196
21. Erdem B, Hunsicker RA, Simmons GW, Sudol ED, Dimonie VL, El-Aasser MS (2001) XPS and FTIR surface characterization of TiO_2 particles used in polymer encapsulation. Langmuir 17:2664–2669
22. Bharti B, Kumar S, Lee H-N, Kumar R (2016) Formation of oxygen vacancies and Ti^{3+} state in TiO_2 thin film and enhanced optical properties by air plasma treatment. Sci Rep 6:32355
23. Jing L, Xin B, Yuan F, Xue L, Wang B, Fu H (2006) Effects of surface oxygen vacancies on photophysical and photochemical processes of Zn-doped TiO_2 nanoparticles and their relationships. J Phys Chem B 110:17860–17865
24. Vempati S, Kayaci-Senirmak F, Ozgit-Akgun C, Biyikli N, Uyar T (2015) Surface ionic states and structure of titanate nanotubes. RSC Adv 5:82977–82982
25. Lear T, Marshall R, Lopez-Sanchez JA, Jackson SD, Klapötke TM, Bäumer M, Rupprechter G, Freund H-J, Lennon D (2005) The application of infrared spectroscopy to probe the surface morphology of alumina-supported palladium catalysts. J Chem Phys 123:174706
26. Dann EK, Gibson EK, Catlow RA, Collier P, Eralp Erden T, Gianolio D, Hardacre C, Kroner A, Raj A, Goguet A, Wells PP (2017) Combined in situ XAFS/DRIFTS studies of the evolution of nanoparticle structures from molecular precursors. Chem Mater 29(17):7515–7523
27. Zhou H, Yang X, Li L, Liu X, Huang Y, Pan X, Wang A, Li J, Zhang T (2016) PdZn intermetallic nanostructure with Pd–Zn–Pd ensembles for highly active and chemoselective semi-hydrogenation of acetylene. ACS Catal 6:1054–1061
28. Karim A, Conant T, Datye A (2006) The role of PdZn alloy formation and particle size on the selectivity for steam reforming of methanol. J Catal 243:420–427
29. Park J-N, McFarland EW (2009) A highly dispersed Pd–Mg/SiO_2 catalyst active for methanation of CO_2. J Catal 266:92–97
30. Stiles AB, Chen F, Harrison JB, Hu X, Storm DA, Yang HX (1991) Catalytic conversion of synthesis gas to methanol and other oxygenated products. Ind Eng Chem Res 30:811–821
31. Makin EC, Okamoto KK (1980) Process for methanol production, in. Google Patents
32. Bahruji H, Bowker M, Jones W, Hayward J, Ruiz Esquius J, Morgan DJ, Hutchings GJ (2017) PdZn catalysts for CO2 hydrogenation to methanol using chemical vapour impregnation (CVI). Faraday Discuss 197:309–324